Inorganic Chemistry
Article

Inorg. Chem. **2010**, *49*, 2193–2201 **2193**
DOI: 10.1021/ic902011v

Two-Step Assembly of Multinuclear Metallacycles with Half-Sandwich Ir, Rh, and Ru Fragments for Counteranion Encapsulation

Guo-Liang Wang, Yue-Jian Lin, Heinz Berke, and Guo-Xin Jin*

Shanghai Key Laboratory of Molecular Catalysis and Innovative Material Department of Chemistry, Fudan University, Shanghai 200433, P. R. China

Received October 12, 2009

Two-step reactions of $[Cp^*M(\mu\text{-}Cl)Cl]_2$ (M = Ir, Rh) and $[(p\text{-cymene})Ru(\mu\text{-}Cl)Cl]_2$ with first AgOTf or $AgPF_6$ and then pyridyl-substituted dionate ligands [3-(4-pyridyl)pentane-2,4-dione (**L_1**), 1-(4-pyridinyl)butane-1,3-dione (**L_2**), 1-(3-pyridinyl)butane-1,3-dione (**L_3**)] resulted in the formation of the hexanuclear 48-membered metallacycles $[(Cp^*Ir)(L_1)]_6\cdot(OTf)_6$ (**1**) and $[(Cp^*Rh)(L_1)]_6\cdot(OTf)_6$ (**2**), the tetranuclear 28-membered metallacycle $[(Cp^*Ir)(L_2)]_4\cdot(OTf)_4$ (**3**), and the 24-membered metallacycle $[(p\text{-cymene})Ru(L_3)]_4\cdot(OTf)_4$ (**4**), as well as the hexanuclear 48-membered metallacycles $\{[(p\text{-cymene})Ru(L_1)]_6(OTf)\}\cdot(OTf)_5$ (**5**) and $\{[(p\text{-cymene})Ru(L_1)]_6(PF_6)\}\cdot(PF_6)_5$ (**6**) showing encapsulation of the counteranions. Compounds **1**−**6** were characterized by single crystal X-ray analyses and revealed that these metallacycles constructed from half-sandwich metal corners and pyridyl-substituted diketone linkers formed large ring structures. In addition, when the couteranions of **5** and **6** were exchanged, the shapes and sizes of the host units $[(p\text{-cymene})Ru(L_1)]_6^{6+}$ underwent some self-adjustment to allow for accommodation of the different anionic guests. Weak hydrogen bonding of the type $C(S)-F(O)\cdots H-C(sp^3)$ and $P-F\cdots H-C(sp^3)$ and electrostatic interactions are considered the basic forces to establish the metallacyclic units in 5 and **6** with anion encapsulation. The found variation in the metallacyclic geometries was explained on the basis of a structural flexibility of the corner fragments, subtle changes in coordination geometries, and changes in the orientation of the coordinate vectors in the given ligands, as well as the dihedral angles between the two binding fragments (the chelate and the monodentate fragments) in the nonplanar ligands.

Introduction

In the past two decades, significant progress was made in the development of effective routes to access organometallic macrocycles and cages, which exhibited properties typical of supramolecular arrangements.[1−9] In 1990, the first case of a metallacycle, the molecular square $[\{Pd(en)(\mu\text{-}4,4'\text{-bipy})\}_4](NO_3)_8$, was discovered, prepared by self-assembly of the *cis*-protected square-planar Pd(II) precursor with two adjacent labile ligands $[Pd(en)(ONO_2)_2]$ (en = ethylenediamine) with a linear linker 4,4′-bipyridine (4,4′-bipy), and was reported by Fujita and co-workers.[1] Since then, metallacycles and cages have been the focus of many directed studies. Ordered

*To whom correspondence should be addressed. Tel.: +86-21-65643776. Fax: +86-21-65641740. E-mail: gxjin@fudan.edu.cn.

(1) Fujita, M.; Yazaki, J.; Ogura, K. *J. Am. Chem. Soc.* **1990**, *112*, 5645.
(2) (a) Caulder, D. L.; Raymond, K. N. *Acc. Chem. Res.* **1999**, *32*, 975. (b) Leininger, S.; Olenyuk, B.; Stang, P. J. *Chem. Rev.* **2000**, *100*, 853. (c) Zangrando, E.; Casanova, M.; Alessio, Enzo. *Chem. Rev.* **2008**, *108*, 4979. (d) Fujita, M.; Tominaga, M.; Hori, A.; Therrien, B. *Acc. Chem. Res.* **2005**, *38*, 371. (e) Holliday, B. J.; Mirkin, A. *Angew. Chem., Int. Ed.* **2001**, *40*, 2022. (f) Han, Y.-F.; Jia, W.-G.; Yu, W.-B.; Jin, G.-X. *Chem. Soc. Rev.* **2009**, *38*, 3419.
(3) (a) Fujita, M. *Chem. Soc. Rev.* **1998**, *27*, 417. (b) Jones, C. *J. Chem. Soc. Rev.* **1998**, *27*, 289. (c) Ni, Z. H.; Tao, J.; Wernsdorfer, W.; Cui, A. L.; Kou, H. Z. *Dalton. Trans.* **2009**, 2788. (d) Pardo, E.; Carrasco, R.; Ruiz-Garcia, R.; Julve, M.; Llort, F.; Munoz, M. C.; Journaux, Y.; Ruiz, E.; Cano, J. *J. Am. Chem. Soc.* **2008**, *130*(2), 576. (e) Slone, R. V.; Yoon, D. I.; Calhoun, R. M.; Hupp, J. T. *J. Am. Chem. Soc.* **1995**, *117*, 11813. (f) Rosenthal, U.; Burlakov, V. V.; Bach, M. A.; Beweries, T. *Chem. Soc. Rev.* **2007**, *36*, 719.
(4) (a) Chen, H.; Ogo, S.; Fish, R. H. *J. Am. Chem. Soc.* **1996**, *118*, 4993. (b) Smith, D. P.; Baralt, E.; Morales, B.; Olmstead, M. M.; Maestre, M. F.; Fish, R. H. *J. Am. Chem. Soc.* **1992**, *114*, 10647. (c) Fish, R. H. *Coord. Chem. Rev.* **1999**, *185*−*186*, 569.
(5) (a) Klausmeyer, K. K.; Rauchfuss, T. B.; Wilson, S. R. *Angew. Chem., Int. Ed.* **1998**, *37*, 1694. (b) Klausmeyer, K. K.; Wilson, S. R.; Rauchfuss, T. B. *J. Am. Chem. Soc.* **1999**, *121*, 2705. (c) Kuhlman, M. L.; Rauchfuss, T. B. *Inorg. Chem.* **2004**, *43*, 430. (d) Boyer, J. L.; Kuhlman, M. L.; Rauchfuss, T. B. *Acc. Chem. Res.* **2007**, *40*, 233.
(6) (a) Severin, K. *Chem. Commun.* **2006**, 3859. (b) Grote, Z.; Scopelliti, R.; Severin, K. *J. Am. Chem. Soc.* **2004**, *126*, 16959. (c) Piotrowski, H.; Severin, K. *Proc. Natl. Acad. Sci. U.S.A.* **2002**, *99*, 4997. (d) Mirtschin, S.; Krasniqi, E.; Scopelliti, R.; Severin, K. *Inorg. Chem.* **2008**, 47. (e) Lehaire, M. -L.; Scopelliti, R.; Piotrowski, H.; Severin, K. *Angew. Chem., Int. Ed.* **2002**, *41*, 1419.
(7) Yamanari, K.; Yamamoto, S.; Ito, R.; Kushi, Y.; Fuyuhiro, A.; Kubota, N.; Fukuo, T.; Arakawa, R. *Angew. Chem., Int. Ed.* **2001**, *40*, 2268.
(8) (a) Han, Y. F.; Jia, W. G.; Lin, Y. J.; Jin, G. X. *Angew. Chem., Int. Ed.* **2009**, *48*, 6234. (b) Han, Y. F.; Lin, Y. J.; Jia, W. G.; Weng, L. H.; Jin, G. X. *Organometallics* **2007**, *26*, 5848. (c) Han, Y. F.; Lin, Y. J.; Weng, L. H.; Berke, H.; Jin, G. X. *Chem. Comm.* **2008**, 350. (d) Han, Y. F.; Lin, Y. J.; Jin, G. X. *Chem. Comm.* **2008**, 1807. (e) Han, Y. F.; Lin, Y. J.; Jia, W. G.; Jin, G. X. *Organometallics* **2008**, *27*, 4088.
(9) (a) Govindaswamy, P.; Süss-Fink, G.; Therrien, B. *Organometallics* **2007**, *26*, 915. (b) Therrien, B.; Süss-Fink, G.; Govindaswamy, P.; Renfrew, A. K.; Dyson, P. J. *Angew. Chem., Int. Ed.* **2008**, *47*, 1. (c) Yan, H.; Süss-Fink, G.; Neels, A.; Stoeckli-Evans, H. *Dalton. Trans.* **1997**, 4345. (d) Govindaswamy, P.; Linder, D.; Lacour, J.; Süss-Fink, G.; Therrien, B. *Chem. Commun.* **2006**, 4691.

Published on Web 02/01/2010

Scheme 1. Synthesis Routes of **1**−**6**

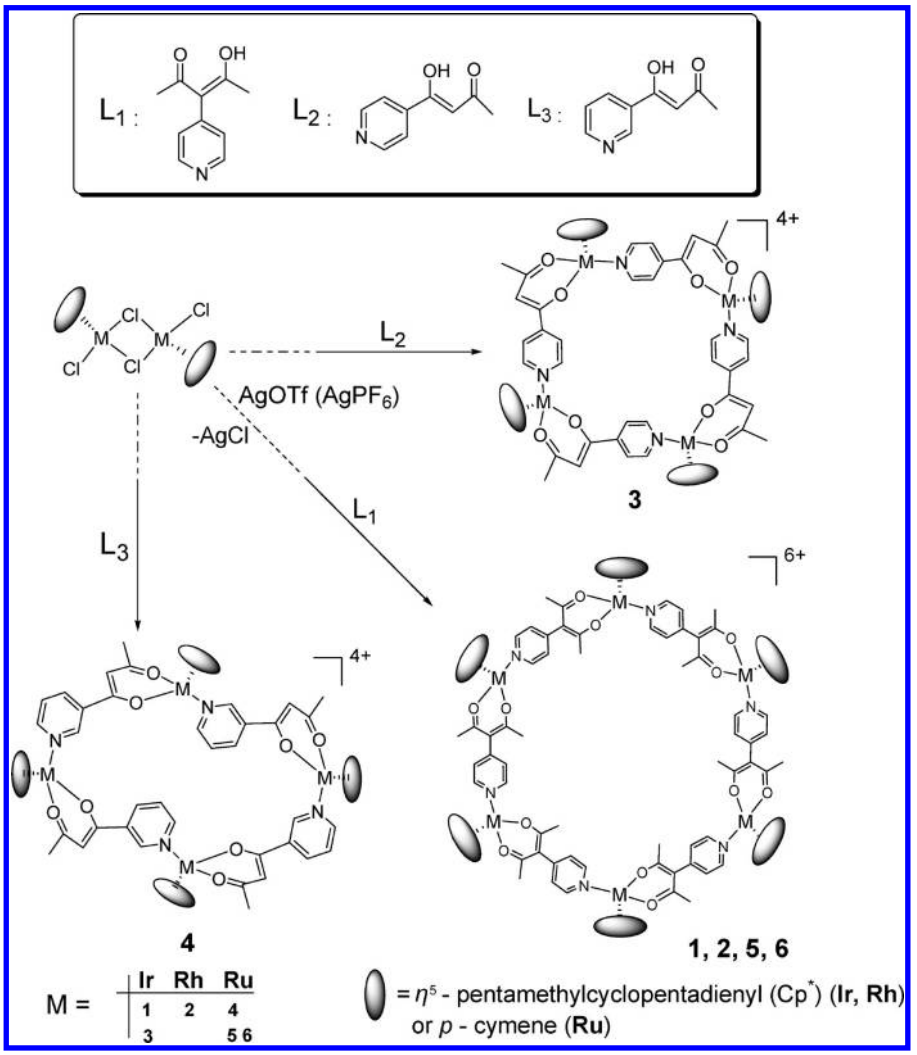

macrocyclic structures were often obtained by rational design using self-assembly principles.[2] Using metal centers as corners and organic linkers in the buildup of such metallacycles led to materials with new properties including guest inclusion,[3a,b] magnetic behavior,[3c,d] luminescence properties,[3e] and catalysis.[3f]

Organometallic half-sandwich complexes have also been widely used as building blocks in the construction of supramolecular complexes.[4−9] Much of this area involved (arene)Ru and (cyclopentadienyl)M (M = Ir, Rh) fragments due to their relative stability and inertness toward substitution reactions and their advantageous basic properties, like solubilities, thermal stabilities, and others needed for flexibility in fine-tuning processes.[6a] Fish and co-workers prepared a series of cationic trinuclear metallacycles by using Cp*Rh fragments as metal corners and deprotonated 9-substituted adenine or hypoxanthine derivatives as linkers, which were capable of aromatic amino acid recognition in aqueous solution.[4] The group of Rauchfuss used cyanometallates such as $[CpCo(CN)_3]^-$ and $[Cp^*Rh(CN)_3]^-$ in combination with other metal complexes derived from dinuclear units like $[(C_6H_3Me_3)Mo(CO)_3]_2$ or $[Cp^*RhCl_2]_2$ or mononuclear ones like $[Cp^*Rh(NCCH_3)_3](PF_6)_2$ and $[Cp^*Ru(NCCH_3)_3]PF_6$ to prepare a series of cubic half-sandwich complexes. In this way, $[\{CpCo(CN)_3\}_4\{Cp^*Rh\}_4]$ was for instance obtained, which showed that the cage acts as a potent receptor for K^+ and Cs^+.[5] Besides this, a series of neutral metallacycles and cages were prepared and characterized by Severin and co-workers, using 2,3-dihydroxypyridine, 3-acetamido-2-hydroxypyridine, 2,3-dihydroxyquinoline, 2,3-dihydroxyquinoxaline, 6-methyl-2,3-phenazinediol, and 3,4-dihydroxy-2-methylpyridine as linkers and (arene)Ru or (cyclopentadienyl)M (M = Ir, Rh) as metal corners.[6] These metallacycles proved to be excellent receptors for Li^+ and Na^+. In particular, the Li^+ containing metallacycles were found to be specific receptors for F^-.[6e] Recently, we and the group of Süss-Fink reported that $(Cp^*MCl_2)_2$ (M = Ir, Rh) and $[(p\text{-cymene})RuCl_2]_2$ complexes can be combined with various organic linkers to build 2- and 3-dimensional molecular structures of squares, prisms, and boxes.[8,9] These complexes looked particularly suited for host−guest interactions and seemed to be prone to including small molecules.[8a]

The half-sandwich Cp*M (M = Ir, Rh) and (*p*-cymene)Ru units acting as corners in various framework geometries are of a basic three-legged piano stool shape, where the piano stool legs can be variably connected with N-, O-, S-, or P-donor ligands.[10] Within this context and in an effort to

(10) (a) Liu, S.; Han, Y. F.; Jin, G. X. *Chem. Soc. Rev.* **2007**, *36*, 1543. (b) Liu, S.; Wang, G. L.; Jin, G. X. *Dalton. Trans.* **2008**, 425. (c) Wang, G. L.; Lin, Y. J. *Inorg. Chem.* **2008**, *47*, 2940–2942.

develop new supramolecular structures, a series of pyridyl-substituted β-diketonate ligands were designed as relatively rigid bridges with a 180° or 120° bridging angle between the η^2-diketonate group and the $N_{pyridyl}$ connecting atoms. These ligands contain both binding sites—a monodentate and a chelating unit, as shown in Scheme 1. They were used as linkers for the construction of coordination polymers.[11] Here, they are recognized as particularly useful linkages in the construction of large ring arrangements.

Herein, we describe the formation of hexanuclear 48-membered metallacycles **1** and **2** with distorted trigonal-antiprismatic metal-based geometries, 28- and 24-membered tetranuclear metallacycles **3** and **4** with distorted tetrahedral and parallelogram type geometries, and hexanuclear 48-membered counteranion encapsulating metallacycles $\{[(p\text{-cymene})Ru(L_1)]_6(OTf)\}\cdot(OTf)_5$ (**5**) and $\{[(p\text{-cymene})Ru(L_1)]_6(PF_6)\}\cdot(PF_6)_5$ (**6**) with trigonal-antiprismatic geometries, respectively (Scheme 1), which were obtained from the two-step reactions of $(Cp^*MCl_2)_2$ (M = Ir, Rh) and $[(p\text{-cymene})RuCl_2]_2$ with initial activation by AgOTf or $AgPF_6$ to create labile coordination sites, and then via reaction with the pyridyl-substituted dionate ligands ($\mathbf{L_1}$, $\mathbf{L_2}$, $\mathbf{L_3}$).

Results and Discussion

Synthesis and Characterization of the Hexanuclear Metallacycles 1 and 2. As shown in Scheme 1, when $(Cp^*MCl_2)_2$ (M = Ir, Rh) was treated with more than four equivalents of AgOTf followed by separation of the AgCl precipitate, the subsequent reactions with the ligands of type $\mathbf{L_1}$ resulted, after recrystallization, in the desired crystalline compounds $[(Cp^*Ir)(L_1)]_6\cdot(OTf)_6$ (**1**) (yield: 51%) and $[(Cp^*Rh)(L_1)]_6\cdot(OTf)_6$ (**2**) (yield: 53%). These products were air- and also thermally stable. Thermal gravimetric analysis (TGA) of **1** revealed no weight loss when heated to 301 °C. The IR spectra showed a strong band at approximately 1571 cm^{-1} for **1** and 1572 cm^{-1} for **2**, owing to the ν(C=O) stretching of the bridging β-diketonate ligands. The ^1H NMR spectra of **1** and **2** in $CDCl_3$ exhibited a sharp singlet at about δ = 1.60 ppm due to the Cp* protons, and, for the two pyridyl protons, at δ = 7.85 and 8.26 ppm for **1** and δ = 7.81 and 8.24 ppm for **2**, indicating the typical chemical shift involvement of the pyridyl-substituted diketonates in metal coordination. Compounds **1** and **2** are soluble in common polar organic solvents, such as CH_2Cl_2, $CHCl_3$, and MeOH.

Synthesis and Characterization of the Tetranuclear Metallacycle 3. A mixture of $(Cp^*IrCl_2)_2$ and more than four equivalents of AgOTf were stirred at room temperature. After filtration of the AgCl precipitate, $\mathbf{L_2}$ was added to the filtrate. $[(Cp^*Ir)(L_2)]_4\cdot(OTf)_4$ (**3**) was obtained after recrystallization in a yield of 67%. The IR spectra showed a strong band at approximately 1585 cm^{-1} assigned to the ν(C=O) stretching vibration of the bridging β-diketonate ligands. The ^1H NMR spectra of **3** exhibited in $CDCl_3$ a sharp Cp* singlet at about δ = 1.63 ppm, and, for the two pyridyl protons, at δ = 8.05 and 8.59 ppm.

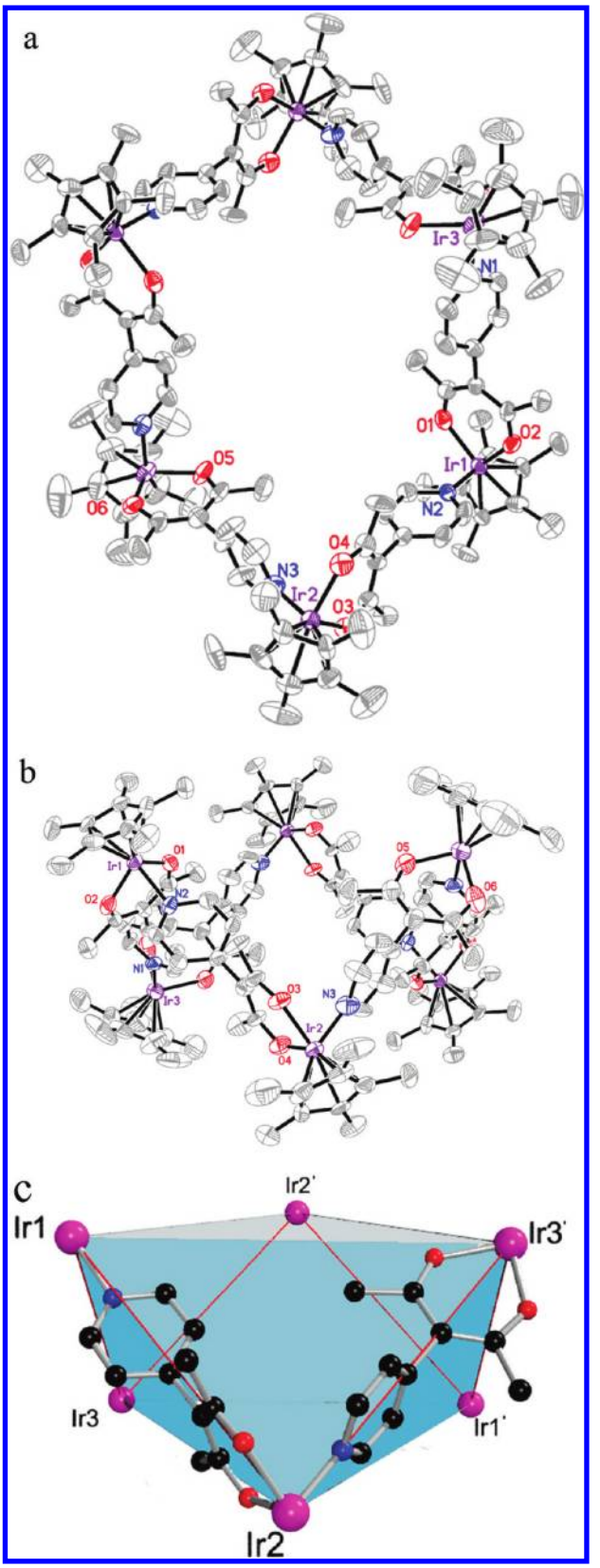

Figure 1. Molecular view of the cationic parts of **1**. Hydrogen atoms have been omitted for clarity. Ellipsoids are shown at 30% probability level. (a) Top view of the metallacycle of **1** with thermal ellipsoids. (b) Side view of the metallacycle of **1** with thermal ellipsoids model. (c) Compound **1** can be described as a distorted trigonal antiprism, in which the metals occupy the vertices, and the pyridine-substituted dione ligands link these vertices along the drawn red lines (the graphical sketch is based on the true crystal structure of **1**. Ir, purple; C, black; O, red; N, blue).

(11) (a) Chen, B.; Fronczek, F. R.; Maverick, A. W. *Chem. Commun.* **2003**, 2166–2167. (b) Zhang, Y.; Chen, B.; Fronczek, F. R.; Maverick, A. W. *Inorg. Chem.* **2008**, *47*(11), 4433–4435. (c) Chen, B.; Fronczek, F. R.; Maverick, A. W. *Inorg. Chem.* **2004**, *43*, 8209–8211. (d) Vreshch, V. D.; Lysenko, A. B.; Chernega, A. N.; Howard, J. A. K.; Krautscheid, H.; Sieler, J.; Domasevitch, K. V. *Dalton. Trans.* **2004**, 2899–2903.

Synthesis and Characterization of the Tetranuclear Metallacycle 4. Initial activation of $[(p\text{-cymene})RuCl_2]_2$ required more than four equivalents of AgOTf followed by separation of the AgCl precipitate. Subsequent reaction with the ligand of type $\mathbf{L_3}$ resulted after recrystallization in the desired crystalline compound $[(p\text{-cymene})Ru(L_3)]_4\cdot(OTf)_4$ (**4**) (yield: 70%). In the ^{1}H NMR spectra, **4** displays signal patterns of δ = 1.39, 2.18, and 2.88 ppm for the proton of the *p*-cymene ligands and δ = 7.41, 7.80, 8.51, and 8.75 ppm for the four unsymmetric 3-pyridyl protons. The IR spectra also showed a strong band at approximately 1587 cm^{-1}, attributed to the ν(C=O) stretching of the bridging β-diketonate ligands.

Synthesis and Characterization of the Hexanuclear Metallacycles 5 and 6. $[(p\text{-cymene})RuCl_2]_2$ was treated with more than four equivalents of AgOTf or $AgPF_6$, followed by separation of the AgCl precipitate. Subsequent reactions with the ligand system $\mathbf{L_1}$ resulted, after recrystallization, in the desired crystalline compounds $\{[(p\text{-cymene})Ru(L_1)]_6(OTf)\}\cdot(OTf)_5$ (**5**) (yield: 48%) and $\{[(p\text{-cymene})Ru(L_1)]_6(PF_6)\}\cdot(PF_6)_5$ (**6**) (yield: 60%). The IR spectra showed a strong band at approximately 1572 cm^{-1} for **5** and 1571 cm^{-1} for **6**, attributed to the ν(C=O) stretching of the bridging β-diketonate ligands. The ^{1}H NMR spectra of **5** (MeOD) and **6** (DMSO−D_6) exhibited typical signal patterns for the protons of the *p*-cymene ligands and the pyridyl protons. Both compounds **5** and **6** are not soluble in $CHCl_3$: **5** was found to be soluble in CH_2Cl_2 and MeOH and **6** in CH_2Cl_2 and DMSO, but not in MeOH.

Description of the Molecular Structures of Complexes. Detailed structural information of **1**−**6** came from single crystal X-ray diffraction analyses. The molecular structures of **1** and **2** turned out to be very similar, therefore compound **1** is prevailingly discussed. Perspective drawings of **1** are shown in Figure 1a,b, and selected bond lengths and angles of **1** and **2** are given in Tables 1 and 2. As shown in Figure 1a,b, the molecular structures revealed a novel hexanuclear metallacycle possessing a 48-membered inner ring. The six η^5-Cp*M fragments are bridged by six 3-(4-pyridyl)pentane-2,4-dionate(L_1) ligands. Each metal center is thus coordinated by two adjacent $O_{diketonate}$ atoms and one $N_{pyridyl}$ atom, forming the mentioned three-legged piano stool. Both compounds **1** and **2** show crystallographic *C*2/*c* symmetry. The edge dimension (Ir···pyridyldionate···Ir) of the metallacycles averages to 9.77 Å. In a simplified view, the geometry of the hexanulear metallacycle can be described as a distorted trigonal antiprism (Figure 1c). The Ir atoms are located at the six vertices of the antiprism with average diagonal lengths of 16.4 Å (Ir···Ir′), and the six edges are occupied by the bridging ligands to result in metal−metal−metal angles of 73.6° (Ir1···Ir2···Ir3′), 92.7° (Ir2···Ir3′···Ir1′), and 90.4° (Ir3′···Ir1′···Ir2′). Furthermore, the top and bottom faces have two small openings, in which the Ir···Ir distances are on the average 13.2 Å and the Ir···Ir···Ir angles are 64.2° (Ir2′···Ir1···Ir3′), 66.5° (Ir1···Ir3′···Ir2′), and 49.3° (Ir3′···Ir2′···Ir1), providing a volume considerably larger than required by the counterions.

Similar to **1** and **2**, compound **3** also bears units with a three-legged piano stool shape, but in this case, four metals are linked by four 1-(4-pyridinyl)butane-1,3-dionate ligands ($\mathbf{L_2}$) to form a 28-membered inner ring (Figure 2). Perspective drawings of **3** are shown in Figure 2a, and selected bond lengths and angles are given in Table 3. Compound **3** can be described as having a distorted tetrahedral geometry for clarity (Figure 2b). Each metal center is located at one of the four vertices of the tetrahedron with the same Ir···L_2···Ir edge dimensions of 9.07 Å and Ir···Ir···Ir angles of 81.9°. Four of the six tetrahedral edges are occupied by $\mathbf{L_2}$ ligands to form a folded square in which the distance between the digonal atoms is 11.9 Å.

Compound **4** connected by $\mathbf{L_3}$ builds up a parallelogram type geometry, which is shown in Figure 3, and selected bond lengths and angles are given in Table 4. The four ruthenium centers form the four vertices of the parallelogram plane with a 24-membered inner ring. As shown in Figure 3b, compound **4** shows average lengths of the edges of 8.52 Å, somewhat shorter than the corresponding length in **3**, as well as M−M−M angles of 102.9° (Ru1···Ru2′···Ru1′) and 77.1° (Ru2′···Ru1···Ru2).

The structures of $\{[(p\text{-cymene})Ru(L_1)]_6(OTf)\}\cdot(OTf)_5$ (**5**) and $\{[(p\text{-cymene})Ru(L_1)]_6(PF_6)\}\cdot(PF_6)_5$ (**6**) were determined by X-ray single crystal diffraction and clearly established the inclusion of the anions in the solid state host of both structures. Perspective drawings of the cations $\{[(p\text{-cymene})Ru(L_1)]_6(OTf)\}^{5+}$ and $\{[(p\text{-cymene})Ru(L_1)]_6(PF_6)\}^{5+}$ are shown in Figure 4, and selected bond lengths and angles of **5** and **6** are given in Tables 5 and 6. As shown in Figures 4 and 5, the compounds **5** and **6** both revealed hexanuclear metallacycles as basic motifs possessing a 48-membered inner ring and containing one of the six counteranions (OTf^-, PF_6^-) centrally. Each metal center is bridged by two binding sites of the ligands $\mathbf{L_1}$, forming the three-legged piano stool like in **1** and **2**. Interestingly, when the counteranions were exchanged

Table 1. Selected Bonds Distances and Angles for **1**

Bond Distances (Å)			
Ir(1)−O(2)	1.993(9)	Ir(1)−O(1)	2.030(8)
Ir(1)−N(2)	2.125(8)	Ir(2)−O(4)	2.057(8)
Ir(2)−O(3)	2.130(7)	Ir(2)−N(3)	2.039(13)
Ir(3)−N(1)	2.100(10)		
Bond Angles (deg)			
O(2)−Ir(1)−O(1)	87.1(3)	O(2)−Ir(1)−N(2)	83.5(3)
O(1)−Ir(1)−N(2)	86.6(3)	O(4)−Ir(2)−N(3)	84.0(4)
O(4)−Ir(2)−O(3)	86.5(3)	N(3)−Ir(2)−O(3)	84.1(4)
O(6A)−Ir(3)−O(5A)	88.7(3)	O(6A)−Ir(3)−N(1)	84.4(4)
O(5A)−Ir(3)−N(1)	83.3(4)		

Table 2. Selected Bonds Distances and Angles for **2**

Bond Distances (Å)			
Rh(1)−N(1)	2.106(8)	Rh(2)−O(1)	2.041(6)
Rh(2)−O(2)	2.075(6)	Rh(2)−N(2)	2.095(7)
Rh(3)−O(4)	2.041(7)	Rh(3)−O(3)	2.076(6)
Rh(3)−N(3)	2.085(9)		
Bond Angles (deg)			
O(6A)−Rh(1)−O(5A)	89.4(3)	O(6A)−Rh(1)−N(1)	86.9(3)
O(5A)−Rh(1)−N(1)	85.0(3)	O(1)−Rh(2)−O(2)	88.7(2)
O(1)−Rh(2)−N(2)	85.5(3)	O(2)−Rh(2)−N(2)	86.3(3)
O(4)−Rh(3)−O(3)	88.9(2)	O(4)−Rh(3)−N(3)	85.0(3)
O(3)−Rh(3)−N(3)	85.9(3)		

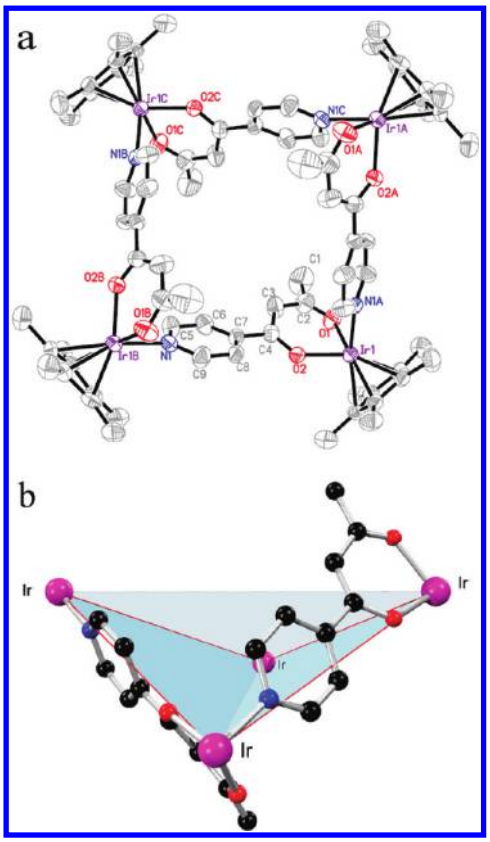

Figure 2. Molecular view of the cationic parts of **3**. Hydrogen atoms have been omitted for clarity. Ellipsoids are shown at the 30% probability level. (a) Top view of the metallacycle of **3** with the thermal ellipsoids model. (b) Compound **3** can be described as having distorted tetrahedral geometry, in which the metals occupy the vertices, and the pyridine-substituted dione ligands connect these vertices along the drawn red lines (the graphical sketch is based on the true crystal structure of **3**. Ir, purple; C, black; O, red; N, blue).

Table 3. Selected Bonds Distances and Angles for **3**

Bond Distances (Å)			
Ir(1)−O(2)	2.083(6)	Ir(1)−O(1)	2.102(8)
Ir(1)−N(1A)	2. 118(8)	C(4)−C(7)	1.470(12)
O(2)−C(4)	1.284(11)	O(1)−C(2)	1.201(12)
Bond Angles (deg)			
O(2)−Ir(1)−O(1)	88.3(3)	O(2)−Ir(1)−N(1A)	82.4(3)
O(1)−Ir(1)−N(1A)	82.8(3)	C(2)−O(1)−Ir(1)	130.6(8)
C(4)−O(2)−Ir(1)	125.5(7)		

in **5** and **6**, the shapes and sizes of the same host units $[(p\text{-cymene})Ru(L_1)]_6^{6+}$ underwent self-adjustment to accommodate the different anionic guests. The geometries of the hexanuclear metallacycles **5** and **6** can be described as trigonal antiprisms (Figure 5). The Ru atoms are positioned at the six vertices, and the six red edges are occupied by the ligands $\mathbf{L_1}$. The edge dimensions (Ru···pyridyldionate···Ru) of compounds **5** and **6** average to 9.77 Å (**5**) and 9.76 Å (**6**), nearly the same distances as in **1** and **2**. However, the host units of **5** and **6** formed obviously by the template effect of the centrally arranged counteranions. The M−M−M angles in **5** are 74.3° (Ru2···Ru1′···Ru3′), 71.9° (Ru1′···Ru2···Ru3), and 74.9° (Ru1′···Ru3′···Ru2′), much larger than the corresponding M−M−M angles in **6**, 64.5° (Ru1′···Ru2···Ru3′),

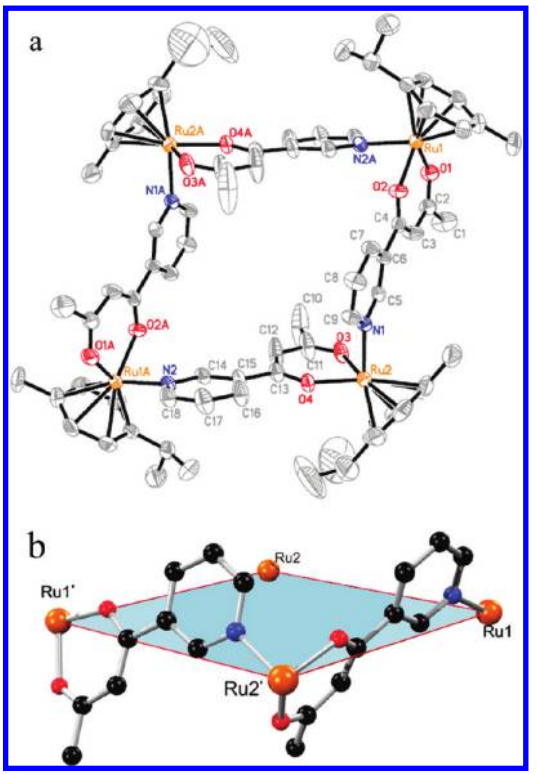

Figure 3. Molecular view of the cation of **4**. Hydrogen atoms have been omitted for clarity. Ellipsoids are shown at the 30% probability level. (a) Top view of the metallacycle of **4** with thermal ellipsoids of the atoms. (b) Compound **4** can be described as having parallelogram geometry, in which the metal centers occupy the vertices, and the pyridine-substituted dione ligands bridge the vertices along the drawn red lines (the graphical sketch is based on the true crystal structure of **4**. Ru, orange; C, black; O, red; N, blue).

Table 4. Selected Bonds Distances and Angles for **4**

Bond Distances (Å)			
Ru(1)−O(2)	2.040(4)	Ru(1)−O(1)	2.049(5)
Ru(2)−O(3)	2.044(5)	Ru(2)−O(4)	2.059(4)
Ru(2)−N(1)	2.106(5)	Ru(1)−N(2A)	2.105(5)
Bond Angles (deg)			
O(2)−Ru(1)−O(1)	89.13(18)	O(2)−Ru(1)−N(2A)	82.73(19)
O(1)−Ru(1)−N(2A)	84.9(2)	O(3)−Ru(2)−O(4)	88.37(18)
O(3)−Ru(2)−N(1)	85.1(2)	O(4)−Ru(2)−N(1)	84.06(18)

64.5° (Ru2···Ru1′···Ru3), and 64.0° (Ru1···Ru3′···Ru2). Furthermore, these different angles result in two distinct top (or bottom) openings of the metallacycles with different sizes and shapes. In compound **5**, these Ru···Ru distances are 11.90 Å (Ru1···Ru2), 11.44 Å (Ru1···Ru3′), and 11.80 Å (Ru2···Ru3′) and the Ru···Ru···Ru angles are 61.6° (Ru1···Ru3′···Ru2), 57.8° (Ru1···Ru2···Ru3′), and 60.7° (Ru2···Ru1···Ru3′). Compared with these openings in **5**, the distances and angles of **6** appear to form an equilateral triangle with three shorter sides [10.34 Å (Ru1′···Ru2′), 10.42 Å (Ru1′···Ru3′), 10.42 Å (Ru2′···Ru3′)] and angles [59.5° (Ru1′···Ru3′···Ru2′), 60.3°(Ru1′···Ru2′···Ru3′), 60.3°(Ru2′···Ru1′···Ru3′)]. The host units of **5** and **6** shows that the cavities adjust in shapes and sizes to the needs for accommodation of the anions. Spheric guests, like PF_6^-, apparently induce more symmetric cavities of the corresponding host than ellipsoidally

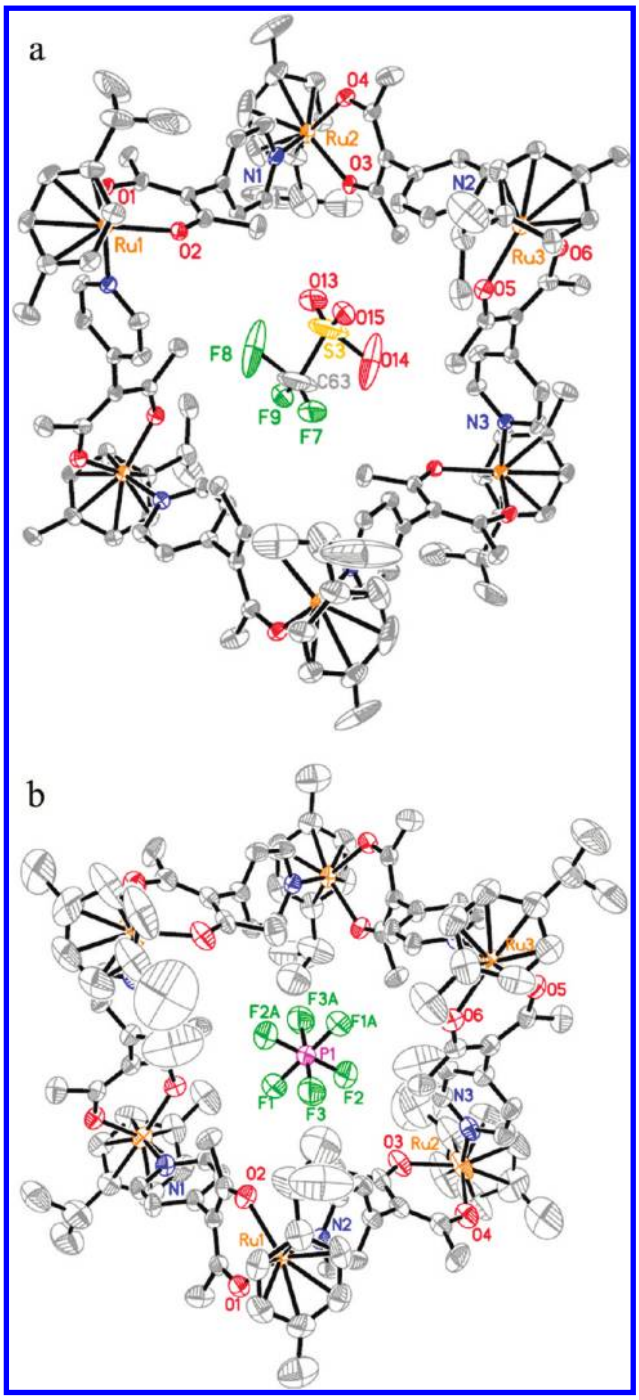

Figure 4. Molecular view of the anion encapsulated in the cations (a) $\{[(p\text{-cymene})Ru(L_1)]_6(OTf)\}^{5+}$ and (b) $\{[(p\text{-cymene})Ru(L_1)]_6(PF_6)\}^{5+}$. Hydrogen atoms were omitted for clarity. Ellipsoids are shown at the 30% probability level.

shaped guests, like OTf^-. The snug fit of the anionic guests within the cavities is manifested in the form of directed hydrogen bonds superimposed by electrostatic interactions between the $[(p\text{-cymene})Ru(L_1)]_6^{5+}$ host and one of the uninegatively charged anions OTf^- or PF_6^-. As shown in Figure 6, the F(O)−C(S) unit of the OTf^- group and the F−P unit of the PF_6^- anion are in close contact with one of the $C(sp^3)$−H hydrogen atoms of the methyl group pointing toward the inside of the cavity. Weak hydrogen bonding in organometallic supramolecular structures has considerably extended the scope for

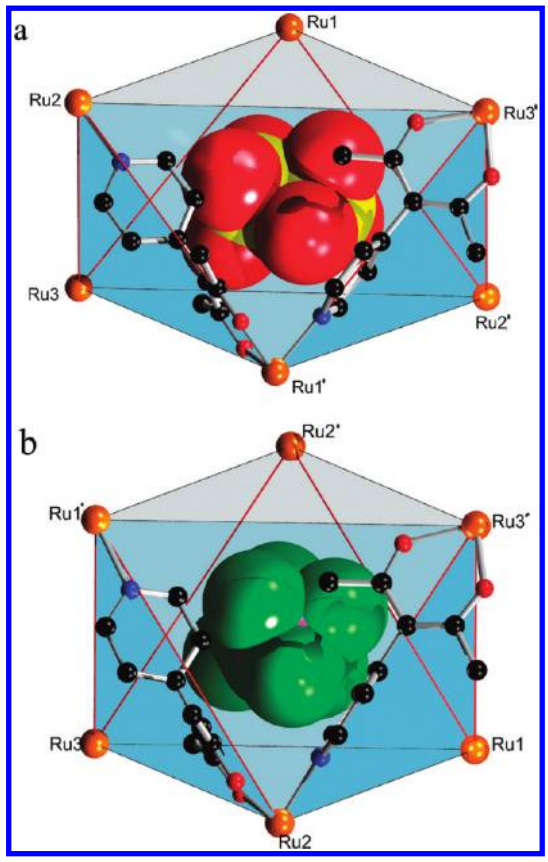

Figure 5. Compounds (a) **5** and (b) **6** can be described as trigonal antiprismatic geometries, in which the metal centers occupy the vertices, and the pyridine-substituted dione ligands connect the corners along the drawn red lines (the graphical sketches are based on the true crystal structures of **5** and **6**. Ru, orange; C, black; O, red; N, blue; F, green; S, yellow; P, purple).

Table 5. Selected Bonds Distances and Angles for **5**

Bond Distances (Å)			
Ru(1)−O(2)	2.040(5)	Ru(1)−O(1)	2.043(4)
Ru(2)−O(4)	2.049(5)	Ru(2)−O(3)	2.054(4)
Ru(2)−N(1)	2.111(6)	Ru(3)−O(5)	2.053(5)
Ru(3)−O(6)	2.063(5)	Ru(3)−N(2)	2.138(5)
Bond Angles (deg)			
O(2)−Ru(1)−O(1)	88.52(17)	O(2)−Ru(1)−N(3A)	83.0(2)
O(1)−Ru(1)−N(3A)	82.25(19)	O(4)−Ru(2)−O(3)	86.69(18)
O(4)−Ru(2)−N(1)	82.8(2)	O(3)−Ru(2)−N(1)	83.9(2)
O(5)−Ru(3)−O(6)	87.56(18)	O(5)−Ru(3)−N(2)	84.32(19)
O(6)−Ru(3)−N(2)	81.4(2)		

Table 6. Selected Bonds Distances and Angles for **6**

Bond Distances (Å)			
Ru(1)−O(1)	2.060(5)	Ru(1)−O(2)	2.065(5)
Ru(1)−N(2)	2.141(6)	Ru(2)−O(3)	2.049(6)
Ru(2)−O(4)	2.078(7)	Ru(2)−N(3)	2.115(6)
Ru(3)−O(5)	2.049(5)	Ru(3)−O(6)	2.057(5)
Bond Angles (deg)			
O(1)−Ru(1)−O(2)	85.4(2)	O(1)−Ru(1)−N(2)	83.2(2)
O(2)−Ru(1)−N(2)	85.1(2)	O(3)−Ru(2)−O(4)	87.2(2)
O(3)−Ru(2)−N(3)	84.6(2)	O(4)−Ru(2)−N(3)	82.5(3)
O(5)−Ru(3)−O(6)	86.6(2)	O(5)−Ru(3)−N(1A)	82.4(2)
O(6)−Ru(3)−N(1A)	83.5(2)		

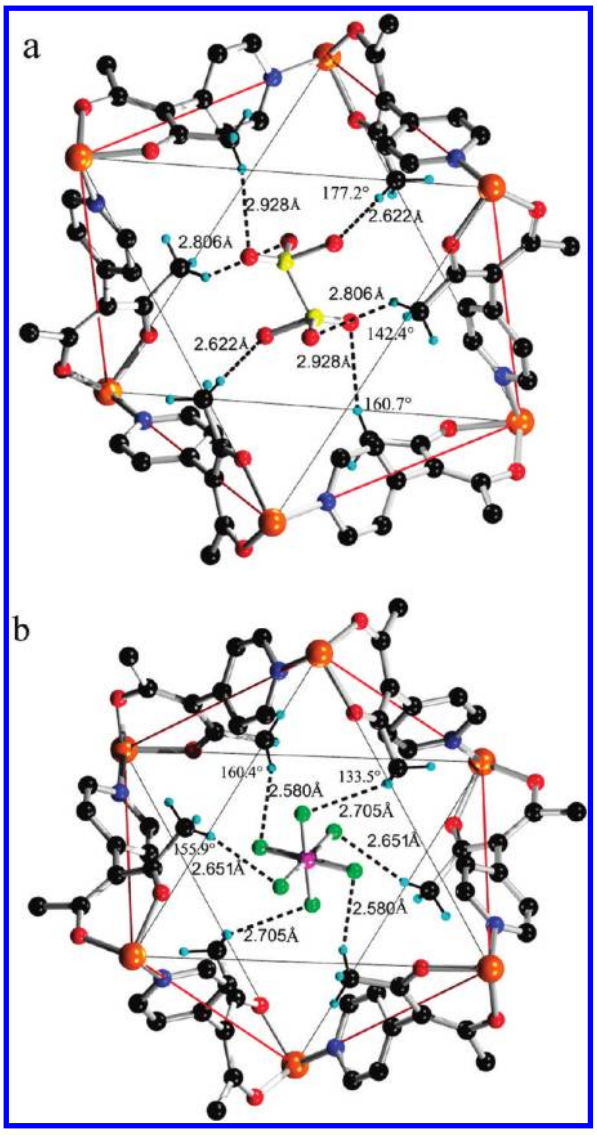

Figure 6. (a) F(O)···H and (b) F···H distances and hydrogen bonding angles in (a) F(O)···H−C and (b) F···H−C occurring between the central anionic guests and the hexanuclear hosts (the graphical sketches are based on the true crystal structures of **5** and **6**; Ru, orange; C, black; O, red; N, blue; F, green; S, yellow; P, purple; H, light blue).

tuning within this class of compounds.[12] The F(O)···H and F···H hydrogen bonding distances and the angles in F(O)···H−C and F···H−C are also presented in Figure 6. Although this type of hydrogen bonding is expected to be weak, the forces are apparently large enough to preclude disorder of the central anions. We consider that cooperation between the hydrogen bonds and the electrostatic forces go together to stabilize the metallacycles of **5** and **6** along with counteranion encapsulation.[13]

Reasoning for the Observed Geometries. Several general attempts have been made to explain the term "self-assembly" in order to understand supramolecular structures and to design structures on a rational basis.[2] Generally speaking, the metal coordination geometry and the

(12) (a) Desiraju, G. R. *Acc. Chem. Res.* **2002**, *35*, 565–573. (b) Steiner, T. *Angew. Chem., Int. Ed.* **2002**, *41*, 48–76. (c) Braga, D.; Grepioni, F.; Desiraju, G. R. *Chem. Rev.* **1998**, *98*, 1375–1405.

(13) Beer, P. D.; Gale, P. A. *Angew. Chem., Int. Ed.* **2001**, *40*, 486–516.

Chart 1. Geometries of the Metallacycles Created from the Combination of Half-Sandwich Metal Corners and the Ditopic Building Ligands with Various Predetermined Coordinate Vectors

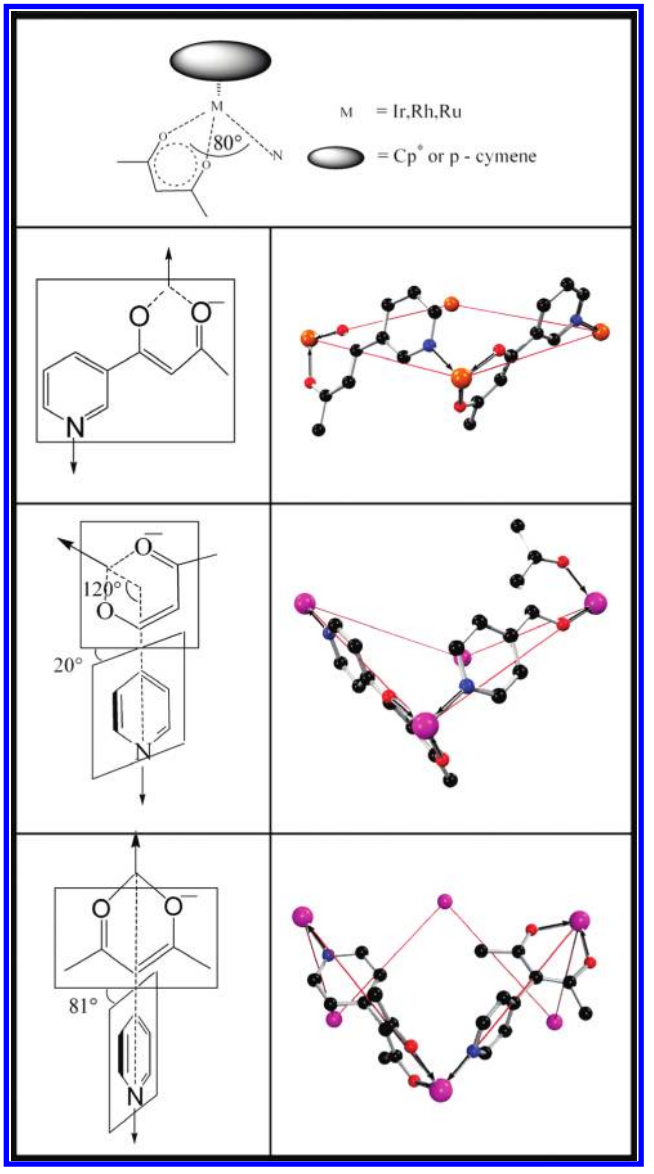

orientation of the interacting sites in the given ligand types govern the sizes and shapes of the resulting structures.[2a,b] The half-sandwich metal corners of this paper are 3-fold connecting units with 2 + 1 distinction, accommodating one bidentate and one monodentate ligand. The coordination angle between the chelate plane and the M→N vector is about 80° (Chart 1). The coordinate vector (the vector from the coordinating atom of the ligand directed toward the metal center) and the chelate vector (the vector that bisects the chelating group and is directed toward the metal ion) of the ligands as defined by Raymond and Caulder[2a] are additionally demonstrated in Chart 1, as well as the dihedral angles between the two binding fragments. In some early reports, Severin and co-workers found that 9-substituted adeninate derivatives afford trinuclear metallacycles, with their two coordinate vectors approximately rectangular. When the coordinate vectors become >90°, the free adeninate induces formation of much wider angles and the buildup

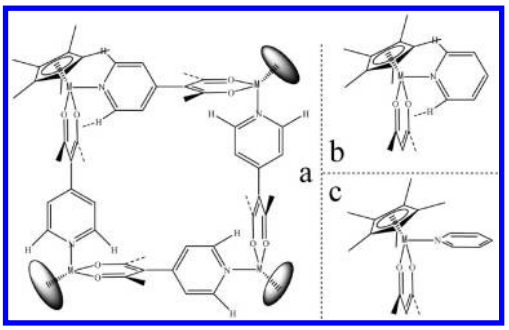

Figure 7. Proposed structure for a tetranuclear metallacycle with $\mathbf{L_1}$.

of molecular squares.[14] In $\mathbf{L_1}-\mathbf{L_3}$, all of the two coordinate vectors are of approximately 120° and 180° and tend to promote the formation of tetranuclear metallacycles in accord with the "rules". The cases of **3** and **4** are explicative with the "rules". Furthermore, when considering the dihedral angles between the two binding units in $\mathbf{L_2}$ and $\mathbf{L_1}$, the dihedral angle of about 20° in $\mathbf{L_2}$ enforces the folded square shape of **3**; the approximately orthogonal dihedral angle in $\mathbf{L_1}$ provides the geometric condition for the formation of a hexanuclear metallacycle with this ligand. This can be further substantiated by the following argument: If $\mathbf{L_1}$ gave a tetranuclear compound with the piano-stool coordination mode of the half-sandwich metal corners and the coordinate vectors of the ligand $\mathbf{L_1}$, the resulting structure would be that of Figure 7a.

As depicted in Figure 7, this structure would be unstable due to repulsion between the two hydrogen atoms of the pyridine group and the adjacent large groups—both the Cp* or *p*-cymene and the acetylacetonate ones. Actually, in all the reported structures mentioned in the Introduction section, besides the structures of **1**−**6**, these piano-stool compounds took the sterically available coordination mode (Figure 4c), not the steric hindrance mode (Figure 4b).

Conclusion

In conclusion, we have described the formation of iridium, rhodium, and ruthenium metal-based hexanulear and tetranuclear macrocycles, which have distorted trigonal antiprismatic, distorted tetrahedral, and parallelogram type geometries directed by varying shapes of the linking pyridyl-substituted dionate derivatives. The resulting structures were found to depend on the metal coordination geometry and the orientation of the coordinate vectors in the given ligands, as well as the dihedral angles between the two binding fragments in nonplanar ligands. The shapes and sizes of the host units $[(p\text{-cymene})\mathrm{Ru}(\mathrm{L_1})]_6^{6+}$ in **5** and **6** self-adjust to encapsulate the different anionic guests. Weak hydrogen bonds of the $\mathrm{C(S)-F(O)\cdots H-C(sp^3)}$ and $\mathrm{P-F\cdots H-C(sp^3)}$ type and Coulombic interactions cooperate to establish the metallacycles in **5** and **6** with anion encapsulation. Further investigations are sought to explore host−guest behavior not only in the solid state but also in solution. On the basis of the derived principles for the construction of supramoelcular structures, we are approaching the preparation of new molecules with designed properties.

(14) Lehaire, M.-L.; Scopelliti, R.; Herdeis, L.; Polborn, K.; Mayer, P.; Severin, K. *Inorg. Chem.* **2004**, *43*, 1609.

Experimental Section

General Considerations. All reactions were carried out under a nitrogen atmosphere using standard Schlenk techniques. All of the solvents were freshly distilled prior to use. CH_2Cl_2 was dried over CaH_2, and CH_3OH was distilled over Mg/I_2. $(Cp^*IrCl_2)_2$, $(Cp^*RhCl_2)_2$, and $[(p\text{-cymene})RuCl_2]_2$ and 3-(4-pyridyl)pentane-2,4-dione ($\mathbf{L_1}$), 1-(4-pyridinyl)butane-1,3-dione ($\mathbf{L_2}$), 1-(3-pyridinyl)butane-1,3-dione ($\mathbf{L_3}$) were prepared according to reported procedures.[15] Infrared spectra were recorded on a Nicolet AVATAR-360IR spectrometer, whereas $^1H\{500\ MHz\}$ NMR spectra were obtained on a Bruker DMX-500 spectrophotometer in proper solvents. Elemental analyses were performed on an Elementar vario EI Analyzer after vacuuming the samples.

Synthesis of $[(Cp^*Ir)(L_1)]_6\cdot(OTf)_6$ (1). A mixture of $(Cp^*IrCl_2)_2$ (0.38 mmol, 300 mg) and AgOTf (1.52 mmol, 390 mg) in MeOH was stirred at room temperature for 3 h. After filtration of AgCl, $\mathbf{L_1}$ (0.85 mmol, 150 mg) was added to the filtrate. The solution was kept stirring for 12 h. Then, the solvent was removed under reduced pressure, producing a yellow solid which was extracted from CH_2Cl_2. The residue solids were recrystallized from CH_2Cl_2/Et_2O to give light yellow crystals of **1** (250 mg, 51% yield). Elemental analysis calcd: C, 38.64; H, 3.86; N, 2.15. Found: C, 38.44; H, 4.00; N, 2.14. ^1H NMR (500 MHz, $CDCl_3$): δ 1.60 (s, $-CH_3$, 15H), 1.79 (s, $-CH_3$, 6H), 7.85 (d, −pyridyl, 2H), 8.26 (b, −pyridyl, 2H). IR (KBr disk): 2918, 1618, 1571, 1425 1384, 1268, 1149, 1102, and 1032 cm^{-1}.

Synthesis of $[(Cp^*Rh)(L_1)]_6\cdot(OTf)_6$ (2), $[(Cp^*Ir)(L_2)]_4\cdot(OTf)_4$ (3), $[(p\text{-cymene})Ru(L_3)]_4\cdot(OTf)_4$ (4), $\{[(p\text{-cymene})Ru(L_1)]_6(OTf)\}\cdot(OTf)_5$ (5), and $\{[(p\text{-cymene})Ru(L_1)]_6(PF_6)\}\cdot(PF_6)_5$ (6). The synthesis of **2**−**6** represents a typical procedure similar to that of **1**. Generally, the products crystallized from CH_2Cl_2/Et_2O within days. For **2** (150 mg, 53% yield), elemental analysis calcd: C, 44.77; H, 4.47; N, 2.49. Found: C, 44.17; H, 4.53; N, 2.45. ^1H NMR(500 MHz, $CDCl_3$): δ 1.62 (s, $-CH_3$, 15H), 1.75 (s, $-CH_3$, 6H), 7.81 (d, −pyridyl, 2H), 8.24 (b, −pyridyl, 2H). IR (KBr disk): 2923, 1618, 1572, 1421, 1265, 1150, and 1031 cm^{-1}. For **3** (214 mg, 67% yield), elemental analysis calcd: C, 37.61; H, 3.63; N, 2.19. Found: C, 37.72; H, 3.77; N, 2.21. ^1H NMR(500 MHz, $CDCl_3$): δ 1.63 (s, $-CH_3$, 15H), 2.29 (s, $-CH_3$, 3H), 7.01 (s, −CH−, 1H), 8.05 (d, −pyridyl, 2H), 8.59 (d, −pyridyl, 2H). IR (KBr disk): 2960, 2921, 1585, 1514, 1436, 1383, 1155, 1030, and 638 cm^{-1}. For **4** (190 mg, 70% yield), elemental analysis calcd: C, 43.95; H, 4.06; N, 2.56. Found: C, 43.88; H, 4.05; N, 2.34. ^1H NMR(500 MHz, $CDCl_3$): δ 1.39 (s, 6H, $-CH(CH_3)_2$), 2.18 (s, 3H, $-CH_3$), 2.88 (m, 1H, $-CH(CH_3)_2$), 2.10 (s, $-CH_3$, 3H), 5.59 (d, C_6H_4, 2H), 5.87 (d, C_6H_4, 2H), 6.80 (s, −CH−, 1H), 7.41, 7.80, 8.51, 8.75 (m, −pyridyl, 4H). IR (KBr disk): 2966, 2927, 1604, 1587, 1517, 1384, 1263, 1155, 1030, and 638 cm^{-1}. For **5** (135 mg, 48% yield), elemental analysis calcd: C, 44.92; H, 4.31; N, 2.50. Found: C, 44.87; H, 4.25; N, 2.56. ^1H NMR(500 MHz, MeOD): δ 1.38 (s, 6H, $-CH(CH_3)_2$), 1.81 (s, 6H, $-CH_3$), 2.88 (m, 1H, $-CH(CH_3)_2$), 2.12 (s, $-CH_3$, 3H), 5.62 (d, C_6H_4, 2H), 5.90 (d, C_6H_4, 2H), 7.90 (d, −pyridyl, 2H), 8.32 (d, −pyridyl, 2H). IR (KBr disk): 2968, 2919, 1611, 1572, 1500, 1426, 1366, 1263, 1165, 1034, 840, 805, and 640 cm^{-1}. For **6** (172 mg, 60% yield), elemental analysis calcd: C, 43.08; H, 4.34; N, 2.51. Found: C, 43.13; H, 4.40; N, 2.43. ^1H NMR(500 MHz, DMSO−D_6): δ 1.36 (s, 6H, $-CH(CH_3)_2$), 1.74 (s, 6H, $-CH_3$), 2.84 (m, 1H, $-CH(CH_3)_2$), 2.10 (s, $-CH_3$, 3H), 5.70 (d, C_6H_4, 2H), 6.01 (d, C_6H_4, 2H), 7.88 (d, −pyridyl, 2H), 8.36 (d, −pyridyl, 2H). IR (KBr disk): 2962, 2920, 1615, 1571, 1532, 1402, 1385, 1342, 1262, 1032, 844, and 637 cm^{-1}.

X-Ray Crystallography. Each crystal was mounted on a glass fiber. Crystallographic measurements were made on a Bruker

(15) (a) Sanders, K. M. *J. Chem. Soc. Perkin. Trans.* **1995**, *1*, 2269. (b) Singh, B. *J. Med. Chem.* **1992**, *35*, 4858.

Table 7. Crystallographic Data for Compounds **1**−**6**

	1	**2**	**3**
empirical formula	$Ir_6C_{126}F_{18}N_6O_{30}S_6H_{150}$	$Rh_6C_{126}F_{18}N_6O_{30}S_6H_{150}$	$Ir_4C_{80}F_{12}N_4O_{20}S_4H_{92}$
temperature (K)	293(2)	293(2)	293(2)
fw	3916.08	3380.34	2554.62
cryst size (mm^3)	0.12 × 0.10 × 0.04	0.25 × 0.15 × 0.12	0.20 × 0.16 × 0.10
cryst syst	monoclinic	monoclinic	tetragonal
space group	*C*2/*c*	*C*2/*c*	*P*4(2)/*n*
a (Å)	47.034(16)	47.13(3)	19.715(12)
b (Å)	11.708(4)	11.671(8)	19.715(12)
c (Å)	35.107(12)	35.01(3)	12.650(11)
α (deg)	90	90	90
β (deg)	128.854(4)	128.995(9)	90
γ (deg)	90	90	90
V ($Å^3$)	15055(9)	14966(19)	4917(6)
Z	4	4	2
ρ_{calcd} (g/cm^3)	1.728	1.500	1.726
μ (Mo Kα) (mm^{-1})	5.456	0.820	5.567
no. of collected reflns	30559	30407	26673
no. of unique reflns	13214	13147	5324
no. of params	755	779	286
goodness of fit	0.910	0.969	0.905
R_1, ωR_2 [$I > 2\sigma(I)$][a]	0.0550, 0.0931	0.0695, 0.1171	0.0497, 0.0986
R_1, ωR_2 (all data)[a]	0.1160, 0.0986	0.1607, 0.1253	0.1406, 0.1138
max./min residual density (e $Å^{-3}$)	1.774/−0.848	0.876/-0.632	1.416/-0.397

	4	**5**	**6**
empirical formula	$Ru_4C_{80}F_{12}N_4O_{20}S_4H_{88}$	$Ru_6C_{126}F_{18}N_6O_{30}S_6H_{144}$	$Ru_6C_{120}F_{36}N_6O_{12}P_6H_{144}\cdot CH_2Cl_2$
temperature (K)	293(2)	203(2)	293(2)
fw	2186.06	3363.25	3423.58
cryst size (mm^3)	0.15 × 0.12 × 0.08	0.20 × 0.12 × 0.10	0.15 × 0.12 × 0.10
cryst syst	triclinic	triclinic	monoclinic
space group	$P\bar{1}$	$P\bar{1}$	*P*2(1)/*m*
a (Å)	10.812(6)	12.6905(13)	15.338(16)
b (Å)	14.418(8)	18.6147(19)	34.43(3)
c (Å)	15.527(9)	18.9997(19)	16.281(17)
α (deg)	90.438(8)	111.8390(10)	90
β (deg)	106.249(8)	107.3050(10)	106.436(14)
γ (deg)	94.686(7)	100.1340(10)	90
V ($Å^3$)	2315(2)	3763.8(7)	8247(15)
Z	1	1	2
ρ_{calcd} (g/cm^3)	1.568	1.484	1.379
μ (Mo Kα) (mm^{-1})	0.821	0.760	0.715
no. of collected reflns	10455	18913	34114
no. of unique reflns	8819	13075	14758
no. of params	555	836	869
goodness of fit	0.940	1.128	0.972
R_1, ωR_2 [$I > 2\sigma(I)$][a]	0.0616, 0.1262	0.0682, 0.1914	0.0760, 0.2024
R_1, ωR_2 (all data)[a]	0.1291, 0.1391	0.0929, 0.2098	0.1194, 0.2212
max./min residual density (e $Å^{-3}$)	1.281/−0.664	1.671/−1.190	1.219/−0.840

[a] $R_1 = \sum||F_o| - |F_c|| / \sum|F_o|$ (based on reflections with $F_o^2 > 2\sigma F^2$). $wR_2 = [\sum[w(F_o^2 - F_c^2)^2]/\sum[w(F_o^2)^2]]^{1/2}$; $w = 1/[\sigma^2(F_o^2) + (0.095P)^2]$; $P = [\max(F_o^2, 0) + 2F_c^2]/3$ (also with $F_o^2 > 2\sigma F^2$).

Smart Apex 100 CCD area detector using graphite monochromated Mo Kα radiation (*λ* = 0.71073 Å) at 293 K. The structures were solved by directed methods (SHELXS-97) and refined on F^2 by full-matrix least-squares (SHELX-97) using all unique data. All non-hydrogen atoms were refined anisotropically. In hexanuclear compounds **1** and **2**, two of the six triflate anions and solvent molecules are strongly disordered and cannot be refined properly. So new data sets corresponding to omission of the disordered anions and solvents were generated with the SQUEEZE algorithm before the structures were refined to convergence. Another triflate anion of the asymmetric unit is also disordered so that the carbon, oxygen, and fluorine atoms of it were refined isotropically. Other non-hydrogen atoms were refined anisotropically. In hexanuclear compound **5**, one of the six triflate anions and solvent molecules are also strongly disordered. Thus, new data sets corresponding to omission of the disordered anions and solvents were generated with the SQUEEZE algorithm before the structures were refined to convergence. Atom C62 was refined isotropically because of nonpositive definition and other non-hydrogen atoms were refined anisotropically. In all compounds, hydrogen atoms which could be found were placed in the geometrically calculated positions with fixed isotropic thermal parameters.

Crystal data, data collection parameters, and the results of the analyses of compounds **1**−**6** are listed in Table 7.

Acknowledgment. This work was supported by the National Science Foundation of China (20721063, 20771028), Shanghai Science and Technology Committee (08DZ2270500, 08DJ1-400103), Shanghai Leading Academic Discipline Project (B108), the National Basic Research Program of China (2009CB825300), and Key Discipline Innovative Training Program of Fudan University.

Supporting Information Available: The crystallographic data for **1**−**6** are available free of charge via the Internet at http://pubs.acs.org.